Mechanical and electrical properties of low SWNT content 3YTZP composites

R. Poyato[1,*], J. Macías-Delgado[1,2], A. García-Valenzuela[1,2], Á. Gallardo-López[1,2], A. Morales-Rodríguez[1,2], A. Muñoz[2], A. Domínguez-Rodríguez[2].

[1] *Inst. Ciencia de Materiales de Sevilla (CSIC-Univ. Sevilla), Avda. Américo Vespucio 49, 41092 Sevilla (Spain).*

[2] *Dep. Física de la Materia Condensada, Univ. de Sevilla, apdo. 1065, 41080 Sevilla (Spain).*

Abstract

Fully dense 3 mol% Y_2O_3-ZrO_2 (3YTZP) composites with low single wall carbon nanotube content (0.5, 1 and 1.5 vol% SWNT) were prepared by colloidal processing and Spark Plasma Sintering. SWNT were distributed at ceramic grain boundaries and also into agglomerates. Characterization of SWNT agglomerates indicated that increase in SWNT vol% does not imply an increase in agglomeration. SWNT agglomerate density was related to the evolution of hardness and fracture toughness with SWNT vol%. Electrical properties of the composites were characterized in a wide temperature range, and percolation threshold was estimated. A model allowing separation of the individual SWNT bundles contribution to resistance from the resistance due to junctions between bundles was proposed for composites with a percolating SWNT network.

Keywords: composites; carbon nanotubes; processing; mechanical properties; electrical properties

[*] Corresponding author.

E-mail address: rosalia.poyato@icmse.csic.es

Phone number: +34 954 48 95 34

FAX number: +34 954 46 06 65

Introduction

Within the past 20 years, the scientific and engineering communities have paid great attention to carbon nanotubes (CNTs) due to their attractive properties. CNTs can show a Young's modulus up to 1.2 TPa, a tensile strength around a hundred times higher than steel and an elevated resilience. They also possess tunable surface properties, well-defined hollow interiors, and can be either metallic or semiconducting depending on diameter and chirality.[1,2] Based on these fascinating properties, many potential applications such as scanning probe tips, drug delivery systems, electronic devices, sensors and actuators, high-strength composites, catalyst support, field emission displays, transparent conducting films, and so on were proposed.[3,4] In these years, both the research articles and patents on this area increased rapidly. Recently, Zhang *et al*.[5] analyzed the publications topic tendency from 2001 to 2011, showing the study of composites with CNTs to be one of the emerging areas, with an increase from 13 to 27% of the total publications. Interest in these composites is based on the possibility of transferring some of the attractive properties of CNTs to the resulting composites[6].

Among advanced ceramics, yttria-doped zirconia is considered a technologically interesting material due to its superior mechanical properties and good ionic conductivity.[7,8] In recent years, several works were devoted to the study of zirconia/CNTs composites, pursuing an enhancement of the mechanical properties. However, up to date, this enhancement has not been clearly demonstrated. A decrease of Vickers hardness when increasing CNT content was reported by different authors,[9-13] even for composites with low CNT vol%.[14-16] Although some authors related this effect to the observed decrease in composite density when increasing CNT content,[9,11] it has been also reported for fully densified composites with SWNT contents up to 10 vol%.[13]

The decreasing trend was also linked to higher presence of agglomerated CNTs[17] in composites with high amount of nanotubes, since it is assumed that agglomeration becomes more relevant due to dispersion difficulties during processing.[18] However, recent investigations on Al_2O_3/SWNT composites have pointed out that the presence of agglomerates does not play a fundamental role on the decrease in hardness.[19] On the contrary, it was rather explained by the presence of higher SWNT quantities at the grain boundaries. The detachment between SWNTs within thick bundles has been pointed out as the origin of the lower fracture toughness obtained for high SWNT content 3YTZP/SWNT composites when compared to monolithic ceramic.[13] In this context, the study of low SWNT vol% composites, in order to asses whether a lower SWNT content at the grain boundaries results in an enhancement of the mechanical properties, appears as a challenge.

The study of the electrical properties of ceramic/CNT composites has recently also come into focus, as adding CNTs to a ceramic matrix also modify the electrical conductivity of the resulting composite. Most of the studies have focused on the analysis of the electrical percolative behaviour,[11,16,20-26] since a step raise in electrical conductivity is the common trend observed in composites once percolation of the CNT network is achieved. Percolation thresholds from 0.64 to 5.5 vol% have been published for composites with alumina or zirconia matrix.[11,16,21-25] This wide range of reported values can be related to the different processing techniques used to prepare the materials. Shin and Liang[22,23] and Fonseca *et al.*[24] reported percolation thresholds of 5.5 and 3 vol% CNTs for 3 mol% Y_2O_3-ZrO_2/MWNT and 8 mol% Y_2O_3-ZrO_2/SWNT composites, respectively. In these studies, composite powders were processed by ball milling the mixture of CNTs and ceramic powder. Recently, composites obtained from powders prepared in a similar way have been shown to present a high amount of CNT

agglomerates,[27] which would result in a lower CNT content at the ceramic grain boundaries than the nominal one. Thus, a higher amount of CNT would be required in order to achieve a percolating network, resulting in an overestimated percolation threshold. These results highlight the need to correlate the CNT agglomerate density and the percolation threshold in ceramic/CNT composites.

Regarding the ac conductivity on ceramic/CNT composites, the published studies are scarce.[24-26] Only Fonseca *et al.*[24] and González-Julián *et al.*[26] reported electrical properties in ac conditions in a wide temperature range. A mixed ionic-electronic conductivity was described for 8 mol% Y_2O_3-ZrO_2/SWNT composites.[24] Charge transport along the nanotube shells and hopping conduction across nanotube-nanotube junctions were suggested as the two contributions to electrical conductivity in Si_3N_4/MWNT composites.[26] To the best of our knowledge, studies on ac conductivity and charge transport contributions in 3YTZP/SWNT composites have not been published up to date.

In this paper, 3 mol% yttria doped zirconia composites containing low SWNT content (0.5, 1 and 1.5 vol%) were prepared by a combination of aqueous colloidal processing and Spark Plasma Sintering, with the aim of obtaining a homogeneous SWNT distribution throughout the ceramic matrix and minimizing the presence of agglomerates. The SWNT agglomerate density was characterized and related to the evolution of hardness and fracture toughness with SWNT vol%. Electrical properties of the composites were characterized in a wide temperature range. Conductivity measurements at room temperature allowed determination of the percolation threshold. Modelling of the impedance properties of the composite with a percolating SWNT network was carried out, and an equivalent circuit which separates the individual

SWNT bundles resistance contribution from the resistance due to junctions between bundles was proposed.

2. Experimental procedure

Raw materials and processing

Monolithic polycrystalline 3YTZP and SWNT/3YTZP composites with different carbon nanotube content (0.5, 1 and 1.5 vol%) were prepared from 3 mol% yttria stabilized tetragonal zirconia powder (3YTZP, 40 nm particle size and 99% purity) supplied by Nanostructured and Amorphous Materials Inc. (Houston, TX) and HIP-co purified SWNTs provided by Carbon Solutions Inc. (Riverside, CA). Acid treatment of the SWNTs was carried out using a mixture of concentrated sulfuric acid (98%) and nitric acid (70%) in the ratio 3:1, with the aim of disentangle and cut the raw SWNTs ropes.[28] This treatment also introduces carboxyl groups on the walls and ends of SWNTs enabling their dispersion in basic medium. SWNTs were suspended in the acid mixture for 24 h at room temperature and the suspension was sonicated for 8 h. SWNTs were collected on ~20 nm pore alumina filter membranes, washed in high purity ethanol for several times and freeze-dried in order to avoid possible re-agglomeration.

Colloidal processing of composite powders with the different SWNT contents was carried out using ammonia solution as a basic medium.[28] Ceramic powder and acid-treated SWNT suspensions were subjected to ultrasonic agitation using a sonication bath before and after mixing. Composite powder blends were dried on a hot plate assisted by stirring, and pH and homogeneity were controlled during the process. Finally, composite powders were homogenized in an agate mortar.

Ceramic sintering

SPS (Model 515S, SPS Dr Sinter Inc., Kanagawa, Japan) was used to sinter the materials in a 15-mm diameter cylindrical graphite die/punch setup in vacuum atmosphere. The sintering processes were carried out at 1250 ºC with a hold time at peak temperature of 5 min, under uniaxial pressure of 75 MPa. Heating and cooling rates were 300 and 50 °C/min, respectively. Bulk densities were measured using Archimedes' method, with distilled water as immersion medium. Theoretical density values for composites were calculated by the rule of mixtures assuming density values of 6.10 $g \cdot cm^{-3}$ for 3YTZP and 1.80 $g \cdot cm^{-3}$ for SWNTs.

Microstructural, mechanical and electrical characterization

Structural integrity of SWNTs in the composites after SPS sintering was assessed by Raman spectroscopy on fracture surfaces using a dispersive microscope (Horiba Jobin Yvon LabRam HR800, Kyoto, Japan) equipped with a 20 mW He-Ne green laser (532.14 nm). The microscope used a 100x objective and a confocal pinhole of 100 μm. The Raman spectrometer was calibrated using a silicon wafer.

Microstructural studies of composites fracture and polished surfaces were performed by high-resolution scanning electron microscopy (HR-SEM), using a Hitachi S5200 microscope (Hitachi High-Technologies America Inc., USA), to analyze the distribution of SWNTs in the 3YTZP matrix, and to characterize the ceramic grains morphology. Distribution and morphology of SWNT agglomerates were characterized by low magnification conventional SEM (Model JEOL 6460LV, JEOL USA Inc., MA, USA). Cross section slices, i.e. surfaces parallel to the SPS pressing direction were polished with diamond paste up to 1 μm for morphological studies. Additionally, polished surfaces devoted to characterize the 3YTZP grains were thermally etched at 1200 °C for 20 min in air to reveal grain boundaries. The morphology characterization

was made measuring 200 grains or agglomerates, respectively, to obtain the equivalent planar diameter as size parameter, d (or D)=2(area/π)$^{1/2}$, and the shape factor, f (or F)=(4π·area)/(perimeter)^2. Standard deviation of distributions was also evaluated. Hereafter, lowercase letters will refer to 3YTZP grains parameters and uppercase letters to agglomerates ones. Agglomerate surface density was evaluated from the area fraction covered by them in low magnification SEM micrographs. *ImageJ* software was used for morphological analysis.

Vickers indentation tests were carried out to evaluate the hardness and fracture toughness of sintered 3YTZP and composites at room temperature. Tests were performed on sample surfaces polished to 1 μm diamond paste using a Vickers indenter with a range of loads up to 2 kgf (Duramin Struers, Germany). Twelve indents were made on each sample avoiding boundary effects (i.e. keeping the appropriate distance from sample edges and between indentations marks) and were analyzed using a confocal microscope LEICA DCM 3D. Vickers hardness, H_v, was calculated from the indentation load, P, and the diagonal of Vickers imprints, a: H_v=1.854(P/a^2).

Fracture toughness, K_{IC}, was calculated by using the equation given by Anstis *et al*.[29] where c is the crack length measured from the centre of the imprint and E the elastic modulus. **The crack length was measured 24 h after the indentation, once the cracks were fully developed.**

$$K_{IC} = 0.016\left(\frac{E}{H_v}\right)^{1/2}\left(\frac{P}{c^{3/2}}\right) \quad (1)$$

Electrical characterization was carried out by Impedance Spectroscopy using an Agilent 4294A analyzer in the frequency range from 100 to 2x10^6 Hz, at temperatures from 25 to 450 °C. Measurements were carried out in argon atmosphere to avoid oxidation of the samples and subsequent degradation of the SWNTs during the process.

Colloidal silver paste was applied on both sides of the samples and electrodes were fired at 600 °C for 30 min under argon flow. Equivalent circuit approach was adopted for the data analysis with fitted curve using Z-view software and equivalent circuit model.

3. Results and discussion

3.1 Microstructural characterization

Table 1 displays the density values together with the global results of morphological parameters of as-sintered samples. A full densification was obtained in all the sintered materials. Similar mean grain size (~230 nm) and shape factor (~0.75) were measured in the different composites and no significant differences were observed compared to monolithic zirconia grains, except for slightly narrower size distributions (smaller $\sigma_{<d>}$).

Fig. 1 shows the Raman spectra measured in the composites, monolithic 3YTZP ceramic and as-received SWNTs. The composites spectra show SWNT characteristic radial breathing mode (RBM) band near 150–200 cm^{-1} and G-band near 1500–1600 cm^{-1}. **In the G-band it can be observed the lower-frequency broad shoulder centred around 1570 cm^{-1} (Breit-Wigner-Fano or BWF lineshape), which is characteristic of metallic SWNT[28]**. The composites spectra are very similar to the SWNT spectrum before processing of the composites, clearly confirming the absence of significant damage to SWNTs during powder processing and sintering. **A G-band shift towards higher frequencies, by ~20 cm^{-1}, is observed in the three composites, which can be attributed to residual stresses in the SWNTs imposed by the constraining ceramic matrix[28].** D-band (centred on 1350 cm^{-1}), associated to disordered graphite and crystalline defects, is also observed. I_D/I_G ratio calculations give similar values for the three composites (6.6, 6.5 and 7.2% for 0.5, 1 and 1.5 vol%

SWNT, respectively) pointing to a similar amount of crystalline defects in the nanotubes. On the other hand, peaks at 165, 260, 320, 465, 610, and 643 cm^{-1} are observed in the spectra acquired in the composites, corresponding to the six Raman bands theoretically predicted for tetragonal zirconia.[30]

HR-SEM micrographs of characteristic fracture surfaces of the composites are presented in Fig. 2. SWNT bundles are located at the ceramic grain boundaries and debonded CNTs from the matrix can also be observed. Whereas the 3YTZP grains surrounded by SWNT bundles are scarce in the composite with 0.5 vol% SWNT (fig 2(a)), the amount of SWNT bundles at the grain boundaries increases in the composites with higher SWNT vol% (figures 2(b) and 2(c)). CNTs are mainly well distributed on the 3YTZP matrix; however, some agglomerates are also found in these high-resolution observations. The presence of these agglomerates or clusters has been previously reported in CNT/ceramic matrix composites.[13,19,27,31,32]

Low-magnification SEM micrographs (Fig. 3) illustrate the arrangement and morphology of SWNT agglomerates in the studied composites. The maximum agglomerate size ranges from 30 to 60 μm (Table 2), which is similar to previously published values for Al_2O_3/MWNT composites also prepared by colloidal processing[32]. Although it is assumed that the tendency of forming agglomerates is due to Van der Waals interactions between nanotubes, they are not expected to lead to such important agglomerate sizes in composites with a rather low SWNT content[32] as in this study. Other forces that might play a key role in the behaviour of the 3YTZP/SWNT powder mixtures have been suggested, and it was shown from thermodynamic considerations that long, thin rods mixed with spheres can induce phase separation and demixion[32].

Similar mean agglomerate size, about 7–9 μm, and a marked elongation (F ~ 0.45) are found for the three composites. These morphological characteristics are similar

to those reported by Morales-Rodríguez *et al.*[19] for Al_2O_3/SWNT composites prepared by a similar processing route. These authors showed that SWNT agglomerates are flattened structures strongly aligned on the direction perpendicular to the SPS compression axis.

An increase in the agglomerate surface density ρ_s is observed when increasing SWNT vol% (Table 2). Nevertheless, this fact does not imply an increase of the percentage of the total SWNT content that is agglomerated, A%. Assuming that the area fraction covered by agglomerates in SEM micrographs is equal to its volume fraction in composites ($\rho_s=\rho_v$, Delesse´s principle of stereology), this percentage can be estimated as:

$$A\% = 100\ \rho_v/\text{SWNT vol\%} \quad (2)$$

Despite the increase in agglomerate volume fraction for higher SWNT vol%, similar percentages of agglomerated SWNTs (~ 30%) from the total SWNT content have been found in the three composites. So an increase in SWNT content does not imply an increase in agglomeration.

The SWNT vol% contained in the agglomerates (*A*-SWNT) and distributed at the grain boundaries (*GB*-SWNT) can be directly inferred from agglomerate volume density as:

$$A\text{-SWNT} = \rho_v \quad (3)$$

$$GB\text{-SWNT} = \text{SWNT vol\%} - A\text{-SWNT} \quad (4)$$

As it is shown in Table 2, after colloidal processing and sintering, the real content of nanotubes at the grain boundaries are estimated to be 0.32, 0.74 and 1.1 SWNT vol% for composites with 0.5, 1, and 1.5 nominal SWNT vol%, respectively.

It is interesting to note that lower *A*-SWNT vol% has been achieved in these materials in comparison with Al_2O_3/SWNT composites with similar SWNT content.[19]

Whereas 60% of the SWNT are contained in agglomerates in Al_2O_3/1 vol% SWNT composites,[19] only 26% of SWNT are agglomerated in our 3YTZP composites with the same SWNT content. Although similar processing routines were used in both studies, SWNT freeze-drying after acid-treatment was introduced in the present work with the aim of obtaining a more homogeneous SWNT distribution.[16,33] It is clear that, although it is not possible to reduce the maximum or the mean agglomerate size by freeze-drying the nanotubes instead of drying on a hot plate, a decrease of the percentage of the CNT content that are agglomerated is achieved.

3.2 Mechanical properties

Similar Vickers hardness, H_v, values within the experimental error are obtained for the three composites and the monolithic 3YTZP ceramic (Table 3). To the best of our knowledge, absence of decrease or increase of hardness with increasing CNT content in ceramic matrix composites has only been reported for Al_2O_3 with 1 vol% SWNT composites,[34] since most of the authors report a decrease of hardness, even for composites with low CNT content.[11,14-16] The decreasing trend reported by previous authors for 3YTZP/CNT composites is shown in Figure 4(a). This tendency is usually linked to a decrease in the composite density,[11] an increase in nanotube agglomeration[17] or a weakening of interfacial bonding when the grains are wrapped by CNT and, therefore, the direct contact area and bonding force among grains decrease with increasing CNT content.[12,13] In this study, fully densified composites have been obtained, and the increase in the surface density of agglomerates (Table 2) does not play a fundamental role in the evolution of hardness when increasing SWNT content. Thus, it is clear that the incorporation of low SWNT content in the ceramic matrix minimizes

the SWNT weakening effect on interfacial cohesion between ceramic grains observed in composites with high SWNT content.[13]

Regarding the fracture toughness values, in recent years, there have been different arguments about the validity of the Vickers indentation technique to characterize fracture toughness of CNT-ceramic matrix composites, and it has been suggested that it should be measured by the single-edge notched beam (SENB) method[6,10,35,36]. Some authors have compared the results obtained in ceramic matrix composites using the indentation method with the ones obtained with the SENB test and, although the absolute values of K_{IC} measured by both tests differ (higher values obtained from indentation measurements), a similar trend was observed when measuring using the two techniques[35,36]. Taking this result into account, and considering also the simplicity of the indentation test and the difficulty of obtaining bars for SEBN test from SPS disks in several studies, it has been proposed that, although the K_{IC} values obtained from indentation tests are not fully quantitative, they can be used to compare different compositions tested in a same study, or for comparison purpose with previous works.

Figure 4(b) shows that the obtained K_{IC} data follow a increasing trend for the composites with increasing SWNT vol.%. These values are similar[11,14,15] to previously published results (also obtained from Vickers indentation tests) for 3YTZP composites with low SWNT content. This slight enhancement is consequence of toughening mechanisms present in the composites, such as CNT crack bridging and pull out, and CNT ropes debundling and uncoiling, as described by previous authors.[6]

3.3 Electrical properties

A room temperature conductivity of $6x10^{-6}$ $S \cdot cm^{-1}$ was measured on the composite with 1.5 vol% SWNT (Table 3). On the contrary, monolithic 3YTZP ceramic and composites with 0.5 and 1 vol% SWNT were found to be electrically isolating with a very high room temperature resistivity. The percolation threshold of the carbon nanotubes in the 3YTZP matrix is therefore between 1 and 1.5 vol%. Nevertheless, considering the agglomerates characterization presented above (Table 2), the real percolation threshold would be between 0.74 and 1.1 vol% SWNT (real SWNT content at grain boundaries), values that are comparable to those published in literature for Al_2O_3/MWNT composites (0.64-1 vol%).[20,21,25,32]

The percolation threshold obtained in this study is lower than the published one by Shin and Liang[22,23] for 3YTZP/MWNT composites (~5.5 vol%). This is probably consequence of the processing efforts devoted in this study to minimize the presence of SWNT agglomerates in the composites, which lead to a higher amount of SWNT distributed in the ceramic grain boundaries.

Impedance complex plane plots corresponding to the composite with 1.5 vol% SWNT from room temperature up to 180 ºC, are shown in Fig. 5(a). A single impedance arc can be observed until 180 ºC, when a second arc appears at lower frequency. According to Garrett *et al.*[37] the impedance properties of a SWNT percolating network can be modelled with an equivalent circuit consisting of two R-C elements in series. It has been published that the resistance of the carbon nanotube bundles and the resistance of the junctions between these bundles are the two major contributions to SWNT network resistance,[26,38,39] and it is well established that the resistance across junctions is higher than the resistance through the bundles themselves.[38,39,40] Thus, the lower resistance element in the equivalent circuit model can be assigned to the CNT bundles whereas the higher resistance one can be assigned to the junctions.

In this context, we have modelled the single impedance arc obtained from room temperature to 160 ºC (arc not shown) using an equivalent circuit model (inset in Fig. 5(a)) similar to the described one by previous authors,[37,41] consisting of a R-C element connected in series with a R-CPE (constant phase element). The CPE is generally used to represent a distribution of relaxation times.[42] Fitting parameters are displayed in Table 4. Capacitance values similar to the reported ones for single wall carbon nanotube networks[37] were obtained.

Fig 5(b) shows the evolution of SWNT bundles and junctions resistivities with temperature from room temperature to 160 ºC. A significant difference between them in the whole range of temperatures, with quite higher resistivity values for the junctions, is observed. It has been shown that the junction resistance is strongly dependent on the size of the interconnecting bundles, with the smallest values associated with individual tubes.[39] Thus, the high junction resistivity observed in this study is clearly pointing to junctions involving large diameter bundles or SWNT agglomerates, which will control the overall conductivity properties of the composite, as remarked by previous authors.[39] Decreasing the bundle diameter will reduce the junction resistivity, and will increase the composite conductivity. Future works will be devoted to further SWNT debundling.

It is also observed that whereas the SWNT bundles resistivity is almost constant with temperature, a remarkable decrease of junctions' resistivity is observed with increasing temperature. This behaviour is in good agreement with Sheng's theory of fluctuation-induced electron tunnelling,[43] model that has been successfully applied to describe the primary conduction mechanism across nanotube-nanotube junctions in CNT composites.[23,24] Briefly, a system of SWNTs, such a rope or mat, can be considered as containing many conducting regions separated by small insulating barriers. In such a system, these tiny barriers will be very susceptible to charge

fluctuations, resulting in electric field fluctuations across the tunneling junctions. These fluctuations increase with increasing temperature, and the system conductivity can be described by Sheng's formula

$$\sigma = \sigma_0 \exp\left(\frac{-T_1}{T + T_0}\right) \quad (5)$$

where σ_0 is a preexponential constant, and T_0 and T_1 are the tunneling parameters, which has previously been used to explain conductivity behaviour for carbon nanotube systems.[23,24]

Figure 6 shows impedance complex plane plots corresponding to the composite with 1.5 vol% SWNT from 200 to 400 ºC. Two impedance arcs can be observed, which behave surprisingly in a very different way. Whereas the arc at higher frequency decreases monotonously with temperature, the arc at lower frequency increases up to 350 ºC (arc not shown) and decreases for higher temperatures.

Two impedance arcs were also obtained when characterizing the monolithic 3YTZP ceramic and the composites with 0.5 and 1 vol% SWNT (not shown), the higher frequency one corresponding to conductivity through the ceramic bulk and the lower frequency one corresponding to conductivity through the grain boundaries. However, in these two composites the conductivity evolution with temperature is the typical of an ionic conductor, and both arcs decrease monotonously when increasing temperature, resulting in an increase of conductivity both through the bulk and through the grain boundaries.

In the case of the composite with 1.5 vol% SWNT, the arc at higher frequency would contain the ionic contribution to conductivity through the ceramic bulk and also the electronic one through the SWNT network. The second arc would be related to the ionic conductivity through the grain boundaries, but in this case the fact that a great

fraction of the grain boundaries is covered by SWNTs reduces the ionic conductivity resulting in an increase of the grain boundary resistivity for temperatures up to 350 ºC, and thus, an increase of the arc. For higher temperatures this effect is overcome and the grain boundary conductivity increases with temperature. Equivalent circuit approach of these data in order to obtain conductivity values for the different contributions presents a high complexity and will be addressed in future studies.

Figure 7 shows the Arrhenius plots for total conductivity in the studied composites, together with monolithic zirconia. **Total resistivity was calculated from resistance values obtained from intercepts on the real, Z', axis**. The slope of these diagrams was used to calculate the activation energy of the conducting species (Table 3). For composites with 0.5 and 1 vol% SWNT, as well as monolithic zirconia, a value close to 0.8 eV was obtained. This result is consistent with the activation energy for oxygen vacancy conduction in zirconia-based ceramic oxides.[44,45,46] Thus, these two composites behave as ionic conductors without SWNT percolation. For the composite with 1.5 vol% SWNT, a completely different behaviour was observed, with activation energy of 65 meV, revealing that SWNT contribution to charge transport dominates for temperatures up to 350 ºC. In this case, an ionic-electronic mixed conductor is obtained due to the percolated SWNT network. A similar result was reported for composites of 8 mol% Y_2O_3/ZrO_2 with SWNTs[24], with activation energy of 30 meV.

4. Conclusions

Fully dense 3 mol% yttria doped zirconia matrix composites containing 0.5, 1 and 1.5 vol% SWNT, with equiaxed grain microstructure and almost analogous ceramic grain size (250 nm), were prepared by colloidal processing and SPS. SWNTs were homogeneously distributed at grain boundaries and also into large SWNT agglomerates. Similar agglomerate mean size and shape were found for the three composites.

Increasing SWNT vol% leads to similar percentage of the total SWNT content contained in agglomerates (~30%), and an increasing SWNT content at the grain boundaries.

Similar Vickers hardness and slightly enhanced fracture toughness were obtained for the composites in comparison with the monolithic 3YTZP ceramic. The increase in the surface density of agglomerates does not play a fundamental role in their evolution when increasing SWNT content.

Percolation threshold of the carbon nanotubes in the 3YTZP matrix was estimated to be between 0.74 and 1.1 vol% SWNT corresponding to nominal contents of 1 and 1.5 vol%, respectively. Composites with 0.5 and 1 vol% SWNT behaved as ionic conductors without SWNT percolation, with ~0.8 eV activation energy.

Room temperature conductivity in the composite with 1.5 vol% SWNT revealed the existence of a percolated SWNT network in this material, which presented a mixed ionic-electronic conduction with 65 meV activation energy. Modelling of impedance properties in this composite using an equivalent circuit allowed separation of the individual SWNT bundles contribution to resistance from the resistance due to junctions between bundles. The existence of junctions involving large diameter bundles or SWNT agglomerates resulted in higher junction resistivity in comparison with the SWNT bundles resistivity. The remarkable decrease of junctions' resistivity with increasing temperature up to 160 ºC was successfully described in terms of the fluctuation-induced electron tunnelling across nanotube-nanotube junctions.

Acknowledgements

The authors acknowledge the financial support provided by the Spanish Ministry of Science and Innovation (MAT2012-34217) and Junta de Andalucía (P12-FQM-

1079). Microscopy studies have been performed in facilities belonging to the CITIUS (Universidad de Sevilla).

Figure captions

Figure 1: Raman spectra measured in the composites including the RBM frequency range and the D and G-Bands frequency range. Raman spectra measured in the monolithic 3YTZP ceramic and in the SWNTs have been included for comparison.

Figure 2: HRSEM micrographs of fracture surface of the composites with different SWNT contents (a) 0.5 vol%, (b) 1 vol%, and (c) 1.5 vol%.

Figure 3: SEM micrographs showing the SWNT agglomerate distribution on the cross-sections of composites with different SWNT contents (a) 0.5 vol%, (b) 1 vol%, and (c) 1.5 vol%.

Figure 4: (a) Vickers Hardness and (b) fracture toughness for monolithic 3YTZP and SWNT/3YTZP composites and comparisons with the bibliography values.

Figure 5: (a) Impedance plots acquired in the composite with 1.5 vol% SWNT from room temperature to 180 ºC and (b) SWNT bundles and junctions resistivity in this temperature range. The inset in (a) shows the equivalent circuit used to fit the impedance data.

Figure 6: Impedance plots acquired in the composite with 1.5 vol% SWNT from 200 to 400 ºC.

Figure 7: Arrhenius plots of the electrical conductivity for monolithic 3YTZP and 3YTZP/SWNT composites.

Table 1: Theoretical and relative density and morphological parameters for ceramic grains in monolithic 3YTZP and SWNT/3YTZP composites.

SWNT vol%	ρ_{th} ($g \cdot cm^{-3}$)	ρ_r (%)	<d> (nm)	$\sigma_{<d>}$ (nm)	f
0	6.10	100	215	85	0.75±0.08
0.5	6.08	100	230	80	0.74±0.08
1	6.06	100	215	75	0.73±0.06
1.5	6.04	99.4	240	80	0.76±0.05

Table 2: Surface density of SWNT agglomerates, percentage of carbon nanotube content in agglomerates and at grain boundaries calculated for each composite and morphological parameters of agglomerates.

SWNT vol%	**ρ_s (%)**	**A (%)**	***A*-SWNT vol%**	***GB*-SWNT vol%**	**<D> (μm)**	**$\sigma_{<D>}$ (μm)**	**$D_{máx}$ (μm)**	**F**
0.5	0.18 ± 0.07	36	0.18	0.32	9	7	60	0.4 ± 0.3
1	0.26 ± 0.03	26	0.26	0.74	7	4	30	0.5 ± 0.2
1.5	0.40 ± 0.05	27	0.40	1.10	8	5	40	0.5 ± 0.2

Table 3: Mechanical and electrical properties measured for the studied materials.

SWNT vol%	***Hv* (GPa)**	**K_{IC} ($MPa \cdot m^{1/2}$)**	**σ_{RT} ($S \cdot cm^{-1}$)**	**E_{act} (eV)**
0	12.7±0.4	4.3±0.3	----	0.86±0.02
0.5	13.4±0.3	4.2±0.3	----	0.84±0.08
1	12.6±0.2	4.4±0.2	----	0.76±0.07
1.5	12.9±0.3	4.6±0.3	$6x10^{-6}$	0.065±0.002

Table 4: Equivalent circuit values for the fitting of the impedance properties of the composite with 1.5 vol% SWNT.

T (°C)	ρ_J (kΩ·cm)	C_J (pF)	ρ_B (kΩ·cm)	C_B (pF)
25	158±13	272±3	10.4±0.9	137±3
40	135±11	279±3	9.1±0.8	139±4
60	113±10	293±4	7.8±0.7	139±4
80	93±7	302±4	6.9±0.5	137±4
100	83±6	318±4	6.4±0.5	136±4
120	76±6	340±6	6.5±0.6	132±4
140	70±5	351±5	6.1±0.4	132±4
160	66±6	400±8	6.4±0.6	135±4
180	56±5	475±1	6.6±0.6	128±5

References

[1] Baughman RH, Zakhidov AA, de Heer WA. Carbon nanotubes- the route toward applications. *Science* 2002; **297**: 787-92.

[2] Zhang Q, Huang JQ, Zhao MQ, Qian WZ, Wei F. Carbon nanotube mass production: principles and processes. *Chem Sus Chem* 2011; **4**: 864-89.

[3] Endo M, Strano MS, Ajayan PM. Potential applications of carbon nanotubes. *Top Appl Phys* 2008; **111**: 13-61.

[4] Schnorr JM, Swager TM. Emerging applications of carbon nanotubes. *Chem Mater* 2011; **23**: 646-57.

[5] Zhang Q, Huang JQ, Qian WZ, Zhang YY, Wei F. *Small* 2013; **9**: 1237–65.

[6] Padture NP. Multifunctional composites of ceramics and single-walled carbon nanotubes. *Adv Mater* 2009; **21**: 1767–70.

[7] Deville S, Gremillard L, Chevalier J, Fantozzi G. A critical comparison of methods for the determination of the aging sensitivity in biomedical grade yttria-stabilized zirconia. *J Biomed Mater Res B Appl Biomater* 2005; **72**: 239–45.

[8] Minh NQ. Ceramic fuel cells. *J Am Ceram Soc* 1993; **76**: 563–88.

[9] Duszová A, Dusza J, Tomasek K, Blugan G, Kuebler J. Microstructure and properties of carbon nanotube/zirconia composite. *J Eur Ceram Soc* 2008; **28**: 1023–27.

[10] Garmendia N, Grandjean S, Chevalier J, Diaz LA, Torrecillas R, Obieta I. Zirconia-multiwall carbon nanotubes dense nano-composites with an unusual balance between crack and ageing resistance. *J Eur Ceram Soc* 2011; **31**: 1009–14.

[11] Shin JH, Hong SH. Microstructure and mechanical properties of single wall carbon nanotube reinforced yttria stabilized zirconia ceramics. *Mater Sci Eng A* 2012; **556**: 382–7.

[12] Shen L, Han YH, Xiang C, Tang H, Mukherjee A, Kim S, Bae SI, Huang Q. Phase transformation behavior of ZrO_2 by addition of carbon nanotubes consolidated by spark plasma sintering. *Scripta Mater* 2013; **69**: 736–39.

[13] Poyato R, Gallardo-López A, Gutiérrez-Mora F, Morales-Rodríguez A, Muñoz A, Domínguez-Rodríguez A. Effect of high SWNT content on the room temperature mechanical properties of fully dense 3YTZP/SWNT composites. *J Eur Ceram Soc* 2014; **34**: 1571–79.

[14] Garmendia N, Santacruz I, Moreno R, Obieta I. Slip casting of nanozirconia/MWCNT composites using a heterocoagulation process. *J Eur Ceram Soc* 2009; **29**:1939–45.

[15] Chintapalli RK, Garcia Marro F, Milsom B, Reece M, Anglada M. Processing and characterization of high-density zirconia-carbon nanotube composites. *Mater Sci Eng A* 2012; **549**: 50-9.

[16] Kasperski A, Weibel A, Alkattan D, Estournès C, Turq V, Laurent Ch, Peigney A. Microhardness and friction coefficient of multi-walled carbon nanotube-yttria-stabilized ZrO_2 composites prepared by spark plasma sintering. *Scripta Mater* 2013; **69**: 338–41.

[17] Bakhsh N, Ahmad Khalid F, Saeed Hakeem A. Synthesis and characterization of presureless sintered carbon nanotube reinforced alumina nanocomposites. *Mater Sci Eng A* 2013; **578**: 422-29.

[18] Zapata-Solvas E, Gómez-García D, Domínguez-Rodríguez A. Towards physical properties tailoring of carbon nanotubes-reinforced ceramic matrix composites. *J Eur Ceram Soc* 2012; **32**: 3001-20.

[19] Morales-Rodríguez A, Gallardo-López A, Fernández-Serrano A, Poyato R, Muñoz A, Domínguez-Rodríguez A. Improvement of Vickers hardness measurement on

SWNT/Al_2O_3 composites consolidated by spark plasma sintering. *J Eur Ceram Soc* 2014; **34**: 3801-09.

[20] Rul S, Lefèvre-schlick F, Capria E, Laurent Ch, Peigney A. Percolation of single-walled carbon nanotubes in ceramic matrix nanocomposites. *Acta Mater* 2004; **52**: 1061–67.

[21] Ahmad K, Pan W, Shi SL. Electrical conductivity and dielectric properties of multiwalled carbon nanotube and alumina composites. *Appl Phys Lett* 2006; **89**: 133122.

[22] Shi SL, Liang J. Effect of multiwall carbon nanotubes on electrical and dielectric Properties of yttria-stabilized zirconia ceramic. *J Am Ceram Soc* 2006; **89**: 3533–35.

[23] Shi SL, Lian J. Electronic transport properties of multiwall carbon nanotubes/yttria stabilized zirconia composites. *J Appl Phys* 2007; **101**: 023708.

[24] Fonseca FC, Muccillo R, de Florio DZ, Ladeira LO, Ferlauto AS. Mixed ionic-electronic conductivity in yttria-stabilized zirconia/carbon nanotube composites. *Appl Phys Lett* 2007; **91**: 243107.

[25] Ahmad K, Pan W. Dramatic effect of multiwalled carbon nanotubes on the electrical properties of alumina based ceramic nanocomposites. *Compos Sci Technol* 2009; **69**: 1016–21.

[26] González-Julián J, Iglesias Y, Caballero AC, Belmonte M, Garzón L, Ocal C, Miranzo P, Osendi MI. Multi-scale electrical response of silicon nitride/multi-walled carbon nanotubes composites. *Compos Sci Technol* 2011; **71**: 60–66.

[27] Castillo-Rodríguez M, Muñoz A, Morales-Rodríguez A, Poyato R, Gallardo-López A, Domínguez-Rodríguez A. Influence of the processing route on the carbon nanotubes dispersion and creep resistance of 3YTZP/SWCNTs nanocomposites. *J Am Ceram Soc* 2015; **98**: 645-53.

[28] Poyato R, Vasiliev AL, Padture NP, Tanaka H, Nishimura T. Aqueous colloidal processing of single-wall carbon nanotubes and their composites with ceramics. *Nanotechnol* 2006; **17**: 1770–77.

[29] Anstis GR, Chantikul P, Lawn DB, Marshall DB. A critical evaluation of indentation techniques for measuring fracture toughness: I. direct crack measurement. *J Am Ceram Soc* 1981; **64**: 533–38.

[30] Li M, Feng Z, Xiang G, Ying P, Xin Q, Li C. Phase transformation in the surface region of zirconia detected by UV Raman spectroscopy. *J Phys Chem B* 2001; **105**: 8107–11.

[31] Zhou JP, Gong QM, Yuan KY, Wu JJ, Chen YF, Li CS, et al. The effects of multiwalled carbon nanotubes on the hot-pressed 3 mol% yttria stabilized zirconia ceramics. *Mater Sci Eng A* 2009; **520**:153–7.

[32] Poorteman M, Traianidis M, Bister G, Cambier F. Colloidal processing, hot pressing and characterisation of electroconductive MWCNT-alumina composites with compositions near the percolation threshold. *J Eur Ceram Soc* 2009; **29**: 669–75

[33] Zhang SC, Fahrenholtz WG, Hilmas GE, Yadlowsky EJ. Pressureless sintering of carbon nanotube–Al_2O_3 composites. *J Eur Ceram Soc* 2010; **30**: 1373–80.

[34] Gallardo-López A, Poyato R, Morales-Rodríguez A, Fernández-Serrano A, Muñoz A, Domínguez-Rodríguez A. Hardness and flexural strength of single-walled carbon nanotube/alumina composites. *J Mater Sci* 2014; **49**: 7116-23.

[35] Cho J, Inam F, Reece MJ, Chlup Z, Dlouhy I, Shaffer MSP, et al. Carbon nanotubes: do they toughen brittle matrices?. *J Mater Sci* 2011; 46: 4770–9.

[36] Mazaheri M, Mari D, Razavi Hesabi Z, Schaller R, Fantozzi G. Multi-walled carbon nanotube/nanostructured zirconia composites: outstanding mechanical properties in a wide range of temperature. *Compos Sci Technol* 2011; 71: 939–45.

[37] Garret MP, Ivanov IN, Gerhardt RA, Puretzky AA, Geohegan DB. Separation of junction and bundles resistance in single wall carbon nanotube percolation networks by impedance spectroscopy. *Appl Phys Lett* 2010; **97**: 163105.

[38] Louie SG: Electronic properties, junctions, and defects of carbon nanotubes, in Carbon Nanotubes: Synthesis, Structure, Properties, and Applications, Vol. 80, edited by M.S. Dresselhaus, G. Dresselhaus and P. Avouris (Springer, Berlin, 2001), p. 113.

[39] Nirmalraj PN, Lyons PE, De S, Coleman JN, Boland JJ. Electrical Connectivity in Single-Walled Carbon Nanotube Networks. *Nano Letters* 2009; **9**: 3890-95.

[40] Li C, Thostenson ET, Chou TW. Dominant role of tunneling resistance in the electrical conductivity of carbon nanotube–based composites. *Appl Phys Lett* 2007; **91**: 223114.

[41] Muhlbauer RL, Pruyn TL, Puckett WT, Gerhardt RA. Effect of graphitic filler size and shape on the microstructure, electrical percolation behavior and thermal properties of nanostructured multilayered carbon films deposited onto paper substrates. *J Mater Res* 2014; **29**: 472-84.

[42] Macdonald JR. Impedance spectroscopy. *Ann Biomed Eng* 1992; **20**: 289-305.

[43] Sheng P. Fluctuation-induced tunneling conduction in disordered materials. *Phys Rev B* 1980; **21**: 2180-95.

[44] Guo X, Waser R. Electrical properties of the grain boundaries of oxygen ion conductors: Acceptor-doped zirconia and ceria. *Progr Mater* Sci 2006; **51**: 151-210.

[45] Bernard-Granger G, Guizard C, Surblé S, Baldinozzi G, Addad A. Spark plasma sintering of a commercially available granulated zirconia powder-II. Microstructure after sintering and ionic conductivity. *Acta Mater* 2008; **56**: 4658-72.

[46] Perry NH, Mason TO. Grain core and grain boundary electrical/dielectric properties of yttria-doped tetragonal zirconia polycrystal (TZP) nanoceramics. *Solid State Ionics* 2010; **181**: 276-84.

Figure 1

Click here to download high resolution image

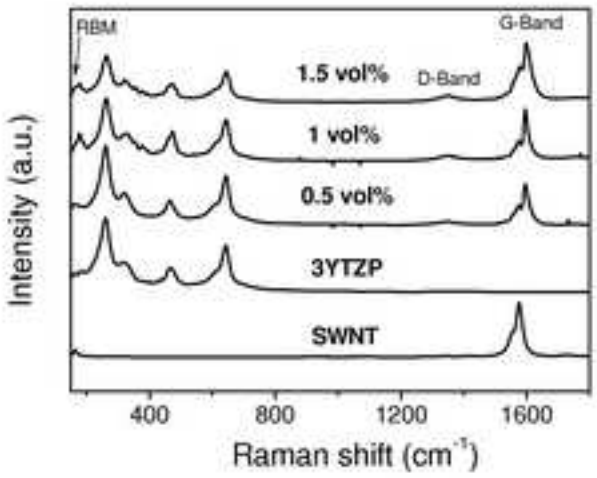

Figure 2

Click here to download high resolution image

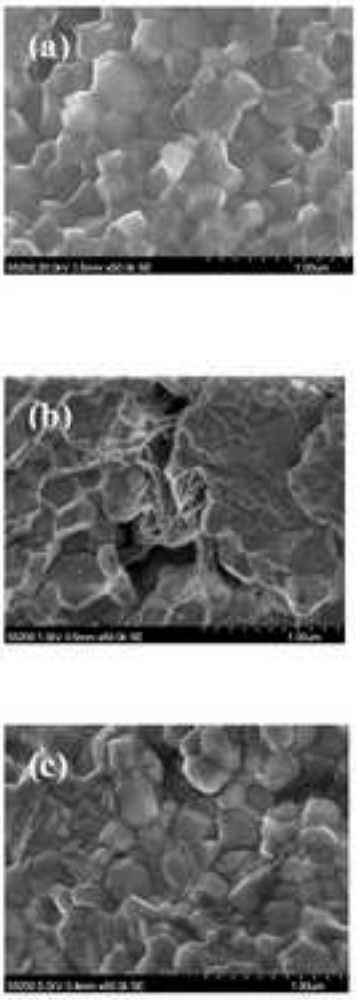

Figure 3

Click here to download high resolution image

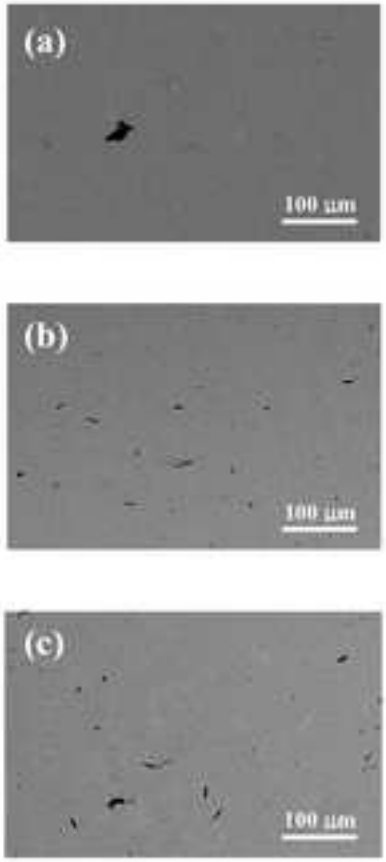

Figure 4

Click here to download high resolution image

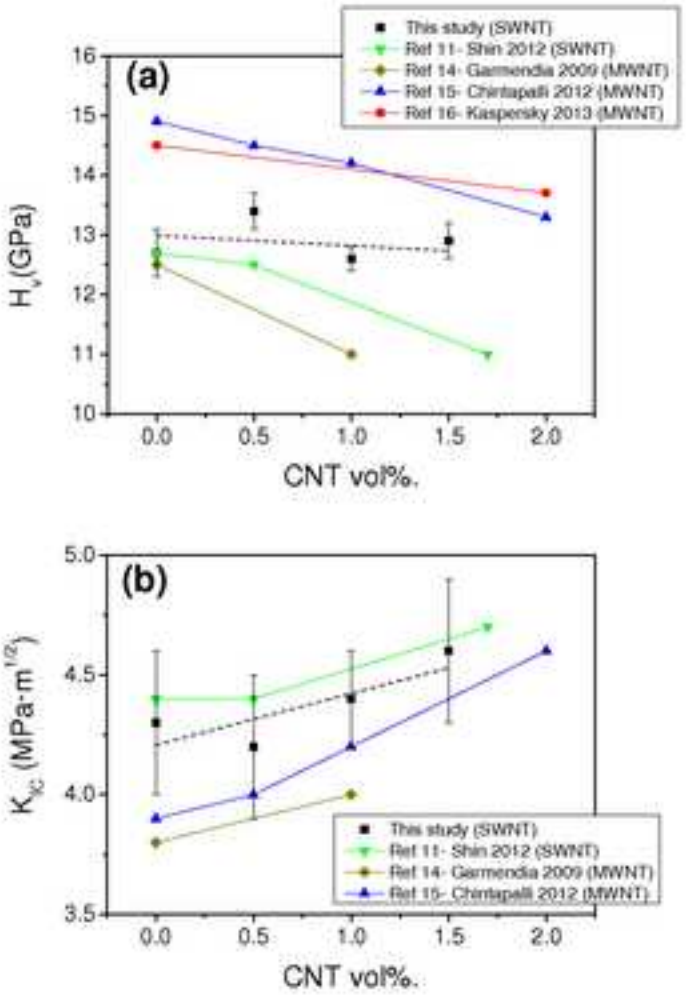

Figure 5

Click here to download high resolution image

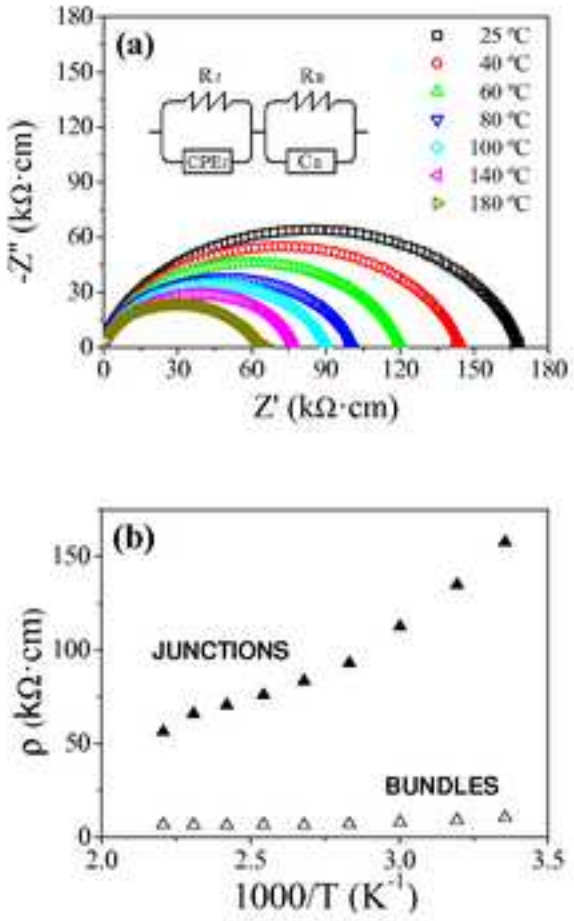

Figure 6

Click here to download high resolution image

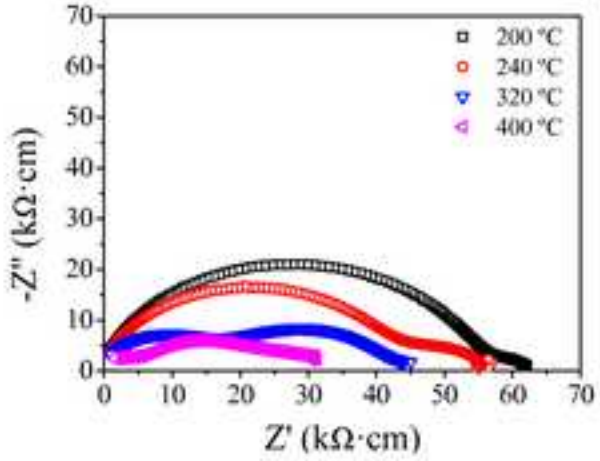

Figure 7

Click here to download high resolution image

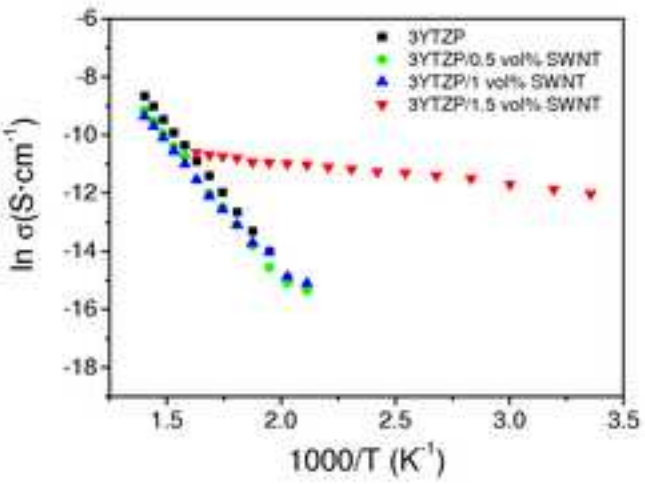

Figure Captions

Figure 1: Raman spectra measured in the composites including the RBM frequency range and the D and G-Bands frequency range. Raman spectra measured in the monolithic 3YTZP ceramic and in the SWNTs have been included for comparison.

Figure 2: HRSEM micrographs of fracture surface of the composites with different SWNT contents (a) 0.5 vol%, (b) 1 vol%, and (c) 1.5 vol%.

Figure 3: SEM micrographs showing the SWNT agglomerate distribution on the cross-sections of composites with different SWNT contents (a) 0.5 vol%, (b) 1 vol%, and (c) 1.5 vol%.

Figure 4: (a) Vickers Hardness and (b) fracture toughness for monolithic 3YTZP and SWNT/3YTZP composites and comparisons with the bibliography values.

Figure 5: (a) Impedance plots acquired in the composite with 1.5 vol% SWNT from room temperature to 180 ºC and (b) SWNT bundles and junctions resistivity in this temperature range. The inset in (a) shows the equivalent circuit used to fit the impedance data.

Figure 6: Impedance plots acquired in the composite with 1.5 vol% SWNT from 200 to 400 ºC.

Figure 7: Arrhenius plots of the electrical conductivity for monolithic 3YTZP and 3YTZP/SWNT composites.